



# A Novel Allosteric Mechanism on Protein–DNA Interactions underlying the Phosphorylation-Dependent Regulation of Ets1 Target Gene Expressions

Masaaki Shiina<sup>1,2</sup>, Keisuke Hamada<sup>1,2</sup>, Taiko Inoue-Bungo<sup>1,†</sup>,  
Mariko Shimamura<sup>1,†</sup>, Akiko Uchiyama<sup>1,†</sup>, Shiho Baba<sup>1</sup>, Ko Sato<sup>1</sup>,  
Masaki Yamamoto<sup>2,3</sup> and Kazuhiro Ogata<sup>1,2</sup>

**1 - Department of Biochemistry, Yokohama City University Graduate School of Medicine, 3-9 Fukuura, Kanazawa-ku, Yokohama 236-0004, Japan**

**2 - RIKEN SPring-8 Center, 1-1-1 Kouto, Sayo-cho, Sayo-gun, Hyogo 679-5148, Japan**

**3 - SPring-8/JASRI, 1-1-1 Kouto, Sayo-cho, Sayo-gun, Hyogo 679-5198, Japan**

**Correspondence to Kazuhiro Ogata:** Department of Biochemistry, Yokohama City University Graduate School of Medicine, 3-9 Fukuura, Kanazawa-ku, Yokohama 236-0004, Japan. [ogata@med.yokohama-cu.ac.jp](mailto:ogata@med.yokohama-cu.ac.jp)  
<http://dx.doi.org/10.1016/j.jmb.2014.07.020>

**Edited by J. Berger**

## Abstract

Cooperative assemblies of transcription factors (TFs) on target gene enhancers coordinate cell proliferation, fate specification, and differentiation through precise and complicated transcriptional mechanisms. Chemical modifications, such as phosphorylation, of TFs induced by cell signaling further modulate the dynamic cooperativity of TFs. In this study, we found that various Ets1-containing TF–DNA complexes respond differently to calcium-induced phosphorylation of Ets1, which is known to inhibit Ets1–DNA binding. Crystallographic analysis of a complex comprising Ets1, Runx1, and CBF $\beta$  at the *TCR $\alpha$*  enhancer revealed that Ets1 acquires robust binding stability in the Runx1 and DNA-complexed state, via allosteric mechanisms. This allows phosphorylated Ets1 to be retained at the *TCR $\alpha$*  enhancer with Runx1, in contrast to other Ets1 target gene enhancers including *mb-1* and *stromelysin-1*. This study provides a structure-based model for cell-signaling-dependent regulation of target genes, mediated via chemical modification of TFs.

© 2014 The Authors. Published by Elsevier Ltd. This is an open access article under the CC BY-NC-ND license (<http://creativecommons.org/licenses/by-nc-nd/3.0/>).

## Introduction

The specificity of transcriptional regulation is determined by transcription factor (TF) complexes, formed on *cis*-acting DNA regulatory elements within enhancer regions [1–3]. The activity and localization of each TF as a component of such regulatory complexes is controlled by various cell signals, via the chemical modification of TFs. TF phosphorylation/dephosphorylation is an important modification, which plays a role in the regulation of nuclear transport [4,5], homo-multimerization [6,7], interactions with coactivators [8,9], and DNA binding [10–12]. However, the effect of TF phosphorylation in the context of functional higher-order TF assemblies on target enhancers remains largely unknown at the atomic level.

The binding specificity of many TFs to their target promoters/enhancers is determined by partnership with other TFs. For example, the *v-ets* erythroblastosis virus E26 oncogene homolog 1 (Ets1) protein regulates target gene expression in cooperation with various partner TFs [13]. Well-characterized Ets1 partners include the runt-related transcription factor 1 (Runx1)–core-binding factor  $\beta$  (CBF $\beta$ ) heterodimer [14], which regulates the *TCR $\alpha/\beta$*  genes encoding the T cell receptor  $\alpha$  and  $\beta$  chains in T cells [15,16]; paired box 5 (Pax5), which regulates the *mb-1* gene encoding the immunoglobulin-associated  $\alpha$  chain in B cells [17–19]; and Ets1 itself, which acts as a homodimer to regulate the *stromelysin-1* (also known as *MMP-3*) gene encoding matrix metalloproteinase 3 in stromal cells [20–22]. These partner TFs are thought to recruit

Ets1 to enhancers, thereby transactivating target genes in a cell-specific manner. Note that, in T cells, the latter two genes, the *mb-1* and *stromelysin-1*, are considered not to be a major target of Ets1.

Ets1 is a member of the Ets family of TFs, which are characterized by a highly conserved DNA binding domain called Ets domain. Previous studies have shown that Ets1 plays crucial roles in a wide variety of biological processes, including hematopoiesis, angiogenesis, apoptosis, and tumor progression and invasion [13]. Ets1 reportedly undergoes  $\text{Ca}^{2+}$ /calmodulin-dependent protein kinase II (CaMKII)-mediated phosphorylation, resulting in Ets1–DNA binding inhibition, which is thought to regulate T cell function [23–26]. We have been studying Ets1-containing, higher-order TF–DNA complexes and the effects of Ets1 phosphorylation induced by calcium signaling on complex formation to better understand the mechanisms underlying cooperative TF assembly.

In the present study, we identify a specific shift in the target gene repertoire following Ets1 phosphorylation. We demonstrate that the regulation of lineage-specific transcription is controlled by the assembly and disassembly of Ets1 and its partner TFs on target enhancers. This process is dynamically controlled by Ets1 phosphorylation, in a manner dependent on both *cis*-elements and specific partner TFs. We also used crystallographic and mutational analyses to compare a complex containing Ets1–Runx1–CBF $\beta$  heterodimer on the *TCR $\alpha$*  enhancer with a complex containing Ets1–Pax5 on the *mb-1* enhancer and an Ets1 homodimer complex on the *stromelysin-1* enhancer. Our findings shed novel insights into the dynamic events underlying Ets1/partner TF-mediated transcription upon cell signaling.

## Results

### Crystal structure of the Ets1–Runx1–CBF $\beta$ –DNA complex

To investigate the mechanism underlying the cooperative binding of Ets1 and Runx1 to the *TCR $\alpha$*  enhancer, we solved the crystal structure of a complex composed of Ets1 (residues 276–441), Runx1 (residues 60–263), CBF $\beta$  (residues 1–141), and a 15-base-pair DNA fragment derived from the *TCR $\alpha$*  enhancer at a resolution of 2.35 Å (Fig. 1a, Fig. S1, and Table S1). The *TCR $\alpha$* / $\beta$  enhancers are known to contain a composite binding site (Fig. S1b), which is reportedly occupied by Ets1 and Runx1 in T cell lines [27]. In the present structure, Ets1 and Runx1 interact from opposite sides of the DNA helix, across a region spanning positions 7–12. Ets1 recognizes DNA major groove using helix 3 (H3) as previously reported and uniquely interacts with DNA minor groove using L1 (Fig. S1d), as will be

described in detail later. Runx1 recognizes DNA major groove using two loops, L3 and L12, and also interacts with minor groove using a loop, L9 (Fig. S1d).

Previous studies indicate that functional cooperativity may be mediated by Ets1–Runx1 protein–protein interaction [15,28,29]. However, crystal structure analysis revealed no direct Ets1–Runx1 interaction using Ets1 (276–441) and Runx1 (60–263) fragments, which contain regions previously reported to be involved in this interaction (Fig. S1). Despite this finding, cooperativity between the DNA interactions of Ets1 and Runx1 fragments was clearly observed (Supplementary Text; Fig. S2).

Ets1 contains an inhibitory module, which flanks the Ets domain (see Fig. 1f for the structure and Fig. S1a for the schematic diagram) [10,30–35]. This module is composed of a hydrophobic core (we refer to as the inhibitory hydrophobic core in this text), surrounded by five  $\alpha$  helices: inhibitory helix 1 (HI-1), inhibitory helix 2 (HI-2), helix 1 (H1), helix 4 (H4), and helix 5 (H5) (Fig. 1j). We then compared the structure of Ets1 within an Ets1–Runx1–CBF $\beta$ –DNA complex to those in DNA complexes with other reported TF partners or in the free state (Fig. 1 and Figs. S3a and 4) [18,19,21,22,34]. In the context of the Ets1–Runx1–CBF $\beta$ –DNA complex, Ets1 assumed a unique conformation in which its regulatory region, including the inhibitory hydrophobic core, was markedly disorganized (Fig. 1e and i, f–h, and j–l). In particular, Tyr329, which is involved in the hydrophobic core in free Ets1 and some Ets1-containing DNA complexes, was flipped outward, leading to a change in the helical phase and position of HI-2 (Fig. 1e–l and Fig. S4), hereafter referred to as HI-2' (Fig. 1e and i and Fig. S4a, e, and i). The formation of the “rearranged” helix HI-2' was accompanied by novel Ets1–DNA interactions between the loop L1 of Ets1 and the DNA backbone, mediated in part by van der Waals contacts between Pro334 and a DNA sugar, as well as a hydrogen bond between Gly333 and a DNA phosphate (Figs. 1e, i, and m and 2a–c). In contrast, the conformation of the inhibitory module of Ets1 in (Ets1)<sub>2</sub>–DNA and Ets1–Pax5–DNA complexes, which do not contain Runx1, resembled that of free Ets1, although HI-1 was disordered [10,19,34,36,37]. Thus, in complexes lacking Runx1, DNA binding of Ets1 elicited only a slight change in the inhibitory hydrophobic core (Fig. 1f–h and j–l and Fig. S4b–d, j, and k).

The DNA conformation within these Ets1-containing complexes also differed, depending on the TF partners bound to sites adjacent to Ets1 (Fig. 1m). In the case of the *TCR $\alpha$*  enhancer, the DNA conformation of the Runx1-bound region within the Ets1–Runx1–CBF $\beta$ –DNA complex was similar to that previously observed in other Runx1-containing DNA complexes (PDB codes 1HJB, 1HJC, and 1IO4) [38]. This suggests that Runx1 defines the specific DNA conformation in the *TCR $\alpha$*  enhancer. The effect of Runx1 binding to DNA extended to the

Ets1-interacting region of the DNA and, remarkably, the DNA conformation defined by Runx1 also affected the structure of the adjacent Ets1 loop L1 (Fig. 1e, i, and m). This is consistent with an observation by Goetz *et al.*, in which DNA-binding cooperativity between Runx1 and Ets1 requires the addition of Runx1 to DNA prior to Ets1 [29]. Meanwhile, in the *mb-1* enhancer, the DNA bound by Pax5 is spatially too close to Ets1, and in the *stromelysin-1* enhancer, DNA bound by the second Ets1 is spatially too distant to Ets1, to interact with loop L1 of Ets1, based on the crystal structures (Fig. 1m).

These observations indicate that, in the case of the Ets1–Runx1–CBF $\beta$  complex formed on the *TCRa* enhancer, an allosteric effect of Runx1 on Ets1, mediated via DNA interaction, is at least in part attributed to the cooperativity of Ets1 and Runx1 for the DNA binding, although other mechanism may further enhance the cooperation.

### Allosteric networks in the Ets1–DNA–Runx1 interaction

Previous studies from our group and others suggested that conformational stabilization of hydrogen bonds between a protein main-chain amide and a DNA phosphate group may be central to the regulation of cooperative DNA binding by TFs [3,38,39]. Stability of a hydrogen bond between a protein main-chain amide and a DNA phosphate is considered to depend on precise positioning and local stability of the protein amide group and/or the DNA phosphate group. To distinguish effects related to the amide and the phosphate groups, we hereafter describe the former as the amide-directed, or A, pathway and the latter as the phosphate-directed, or P, pathway.

Within Ets1-containing DNA complexes, the Leu337 main-chain amide of Ets1 [L337(NH)] invariably forms hydrogen bonds to a DNA backbone phosphate [DNA(PO)], and this hydrogen bond was reportedly facilitated by a macrodipole effect of H1 in Ets family TFs (Fig. S1d) [39]. We therefore predicted that this hydrogen bond may play a critical role in regulating the Ets1–DNA interaction (Fig. 1).

Within the crystal structure of the Ets1–Runx1–CBF $\beta$ –DNA complex, Ets1 and Runx1 interact from opposite sides of the DNA helix, across a region spanning positions 7–12, forming an extensive interaction network through the DNA (Fig. 2a and b and Figs. S1b and S5). At the Ets1–DNA interface, the Ets1 loop L1 recognizes the DNA helix in the minor groove. At the Runx1–DNA interface, the Runx1 loop L9 predominantly recognizes the minor groove, while L12 recognizes the major groove (Fig. 2a and b). The Runx1–DNA interaction involves a combination of van der Waals contacts and hydrogen bonds; the side chain of Val170 of Runx1 forms van der Waals contacts with a DNA sugar and cytosine bases at positions 10 and 11, side chains of Arg174 and Arg177

form hydrogen bonds with guanine bases at positions 10 and 11 and participate in van der Waals contacts with thymine and guanine bases at positions 9 and 10 (Fig. 2a and b), the Asp171 side chain forms hydrogen bonds with cytosine bases at positions 10 and 11, and the side chains of Arg139 and Lys167 and the main-chain amides of Val170 and Gly143 form hydrogen bonds with DNA phosphates at positions 11 and 12 (Fig. 2a and b and Fig. S5). These Runx1–DNA interactions define the DNA structure, thereby enforcing the specific conformation of Ets1 via interactions between the DNA helix and the Ets1 loop L1 (see Discussion). Such an interaction involves van der Waals contacts between Gly333 and Pro334 and DNA sugars at positions 12 and 11, as well as a hydrogen bond between the Gly333 amide and the DNA phosphate at position 12, as previously described. The Ets1 loop L1 is further stabilized intramolecularly by van der Waals contacts involving the Pro334, Tyr329, and Ile335 side chains (Figs. 1e and i and 2a).

Crystallographic analysis of the mutant Ets1(Y329A)–Runx1–CBF $\beta$ –DNA complex revealed that the N-terminal region adjacent to the Ets domain was remarkably disordered. Specifically, contacts between Ets1 loop L1 and the DNA helix were significantly disrupted, highlighting the contribution of the abovementioned interaction network to the maintenance of the specific Ets1 conformation (Fig. S3b and c and Table S1). Because L337(NH) is positioned at the boundary between L1 and H1 in Ets1 (Figs. 1i and 2a), it is suggested that stabilization of L1 by Runx1-bound DNA would enhance Ets1–DNA binding by stabilizing the hydrogen bond between L337(NH) and DNA(PO) (the A pathway) (Fig. 2c and Fig. S6). In addition, the Runx1 Arg80 side chain forms hydrogen bonds with the guanine base at position 8 and makes van der Waals contacts with the thymine base at position 7. Thus, the L337(NH) hydrogen-bonded DNA(PO) is stabilized via G8:C8' base pairing and Arg–DNA base stacking (Fig. 2a and b). This phosphate-directed mode of stabilizing the hydrogen bond between L337(NH) and DNA(PO) (the P pathway) may also enhance Ets1–DNA binding (Fig. 2c and Fig. S6).

It is assumed that the L337(NH)- and DNA(PO)-directed interaction networks (the A and P pathways) extending from Runx1–CBF $\beta$  to the Ets1 L337(NH)–DNA(PO) hydrogen bond via the DNA enhancer establish an “allosteric network” for TF–DNA assembly. In this model, Runx1 likely contributes to the specific DNA recognition of Ets1 by restricting the DNA conformation, which results in a unique interaction between the Ets1 loop L1 and the DNA.

### Robust nature of the interaction network

To examine whether the proposed allosteric network functions in the cooperative binding of

Ets1 and Runx1 to the *TCRa* enhancer, we performed mutational analyses on the residues involved in the A and P pathways using electrophoretic mobility shift assays (EMSA). We first introduced mutations into Ets1 (G333P, P334G, or P334Q) or Runx1 (V170A), which are predicted to largely impair the A pathway, or into Runx1 (R80K), which is predicted to mainly impair the P pathway. The wild-type or mutant Ets1 was then titrated against DNA or the wild-type or mutant Runx1-bound DNA. We also performed crystallographic analysis in parallel, to confirm that neither the G333P mutation in Ets1 nor the V170A mutation in Runx1 affected the Ets domain conformation within the Ets1–Runx1–CBF $\beta$ –DNA complex (Table S1).

As previously reported, Runx1 enhanced Ets1 binding to the *TCRa* enhancer ~10-fold (Fig. 3a and Table S3). The majority of individual Ets1 or Runx1 mutations, each of which impaired only one of the two stabilization pathways, did not appreciably affect the cooperative DNA binding of Ets1 and Runx1. The Ets1 P334G mutation markedly reduced the binding of Ets1 itself (Fig. 3a, Table S3 and Fig. S7), and therefore, the cooperativity between Ets1 and Runx1 could not be assessed for this mutant. In contrast, multiple mutations in Runx1 and/or Ets1 capable of impairing both the A and P pathways clearly reduced the cooperative DNA binding of Ets1 and Runx1 (Fig. 3a and Table S3). This suggests that both

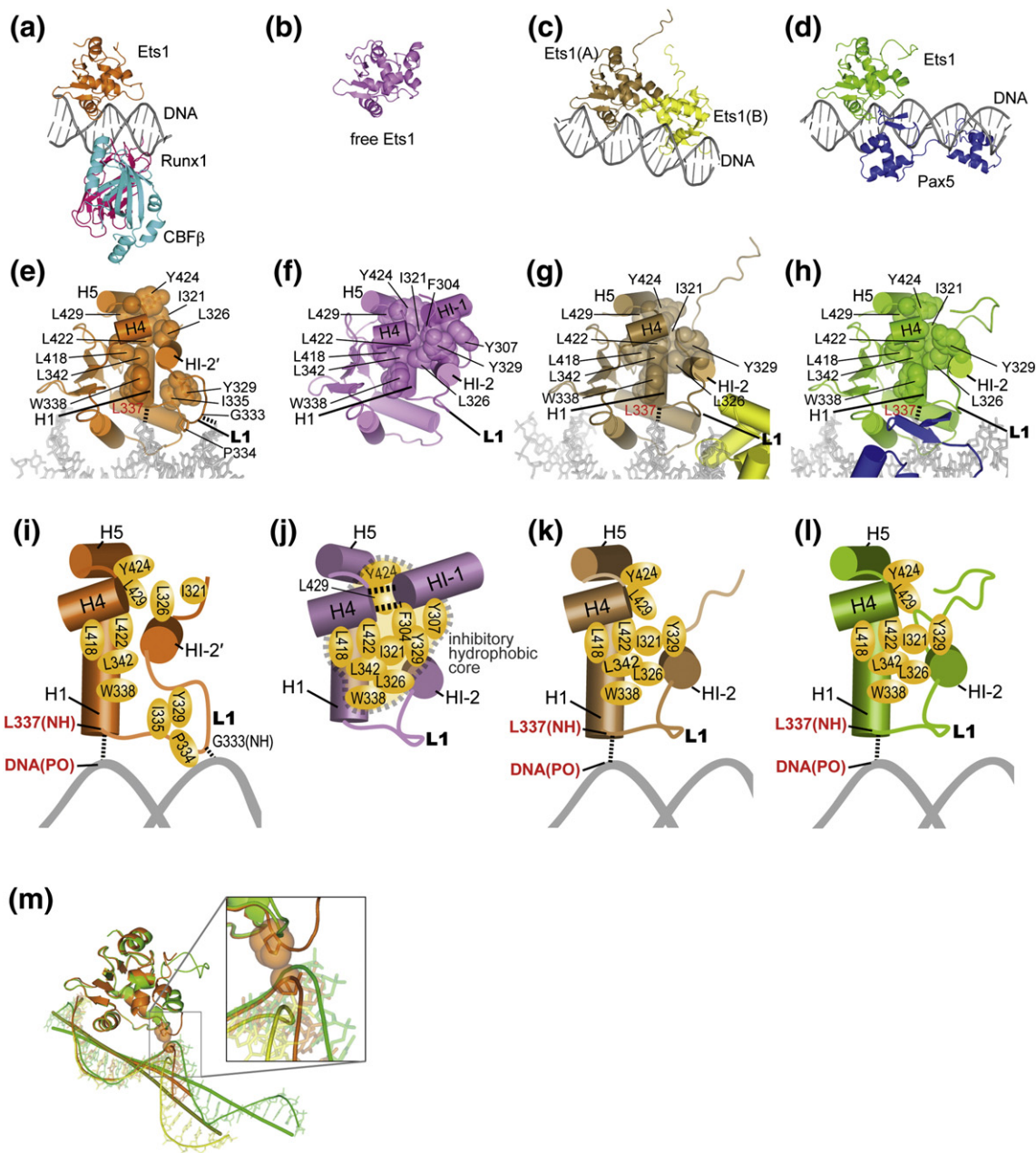


Fig. 1 (legend on next page)

the A and P pathways mediate allosteric regulation and have compensatory functions within the Ets1–Runx1–CBF $\beta$ –DNA complex, increasing the robustness of complex stability. Mutation of other Runx1 residues that interact with the DNA did not appreciably affect the cooperative DNA binding of Ets1 and Runx1, although they significantly reduced the DNA binding of Runx1 itself (Fig. S8).

Previously, Goetz *et al.* reported no involvement of the DNA-mediated effect in the cooperative DNA binding between Ets1 and Runx1, based on the results from EMSA using a nicked DNA. They introduced a single-strand nick in DNA at the critical phosphate group in a composite site of Ets1 and Runx1 to eliminate the DNA-mediated effect. They found that the nick did not affect the cooperativity and concluded that no DNA-mediated effect by Runx1 works [29]. This seems contrary to our results. However, considering that the introduction of the DNA nick would impair the P pathway (Fig. 3a), the effect of the DNA nick, like the R80K mutation, may be compensated by the remaining A pathway on the *TCRa* enhancer.

### Stabilization pathways in other Ets1-containing TF–DNA complexes

We next examined whether the A and P pathways also function in other Ets1-containing TF–DNA complexes. In the (Ets1)<sub>2</sub>–DNA complex formed on the *stromelysin-1* enhancer, two molecules of Ets1, Ets1(A) and Ets1(B), bind to an inverted repeat of the Ets1 binding site in a head-to-head orientation across adjacent DNA grooves (Fig. 1c). This interaction involves the formation of a hydrogen bond and a van der Waals contact between the main chains of Gly333 of Ets1(A) and Asn380 of Ets1(B), as well as between the side chains of Pro334 of Ets1(A) and Lys379 of

Ets1(B) (Fig. 2d and Fig. S6b) [21,22]. These interactions are thought to stabilize the loop L1 and, as a result, L337(NH), via the A pathway. Previous analysis of Ets1 binding to the *stromelysin-1* enhancer revealed that specific Ets1 mutations (G333A, P334A, or N380A) abolish cooperative DNA binding [21,22]. This indicates that the A pathway mediates cooperative binding within the (Ets1)<sub>2</sub>–DNA complex (Fig. 2d and Fig. S6b). No interaction network corresponding to the P pathway was identified in this complex.

Analysis of the Ets1–Pax5–DNA complex formed on the *mb-1* enhancer revealed that the side chain of Gln22 in Pax5 interacts from the major groove with DNA(PO), which is hydrogen bonded to the L337(NH) of Ets1 in the minor groove (Figs. 1d and 2e), thereby stabilizing DNA(PO) via the P pathway (Fig. 2e and Fig. S6c). EMSA analyses revealed that mutation of Ets1 affecting the A pathway (G333P or P334G) did not significantly affect cooperative DNA binding of Ets1 and Pax5 (Fig. 3b and Table S5). Conversely, mutation of Pax5 (Q22A) has been previously shown to significantly impair Ets1 recruitment by Pax5 [40], suggesting that the P pathway is involved in cooperative Ets1 binding in the Ets1–Pax5–DNA complex (Fig. 2e and Fig. S6c).

Taken together, these results suggest that cooperative Ets1 binding within the (Ets1)<sub>2</sub>–DNA complex and the Ets1–Pax5–DNA complex is mediated by the A and P pathways, respectively.

### Resistance to the inhibitory effect of Ets1 phosphorylation on DNA binding

CaMKII-catalyzed phosphorylation of Ets1 in a serine-rich region of the N-terminal extension of HI-1 is known to stabilize the inhibitory hydrophobic core (Fig. 1b, f, and j), resulting in a 50- to 1000-fold reduction in its affinity for DNA [12,23,37,41]. However,

**Fig. 1.** Comparison of Ets1 structures in both free and DNA-complexed states. (a–d) Overviews of the crystal structures of the Ets1–Runx1–CBF $\beta$ –DNA complex (a), free Ets1 (301–440) [(b) PDB code 1R36], the [Ets1 (280–441)]<sub>2</sub>–DNA complex [(c) PDB code 2NNY], and the Ets1 (280–440)–Pax5 (1–149)–DNA complex [(d) PDB code 1MDM]. Ets1 is represented by orange in (a), light purple in (b), brown [Ets1(A)] and yellow [Ets1(B)] in (c), and green in (d).  $\alpha$  Helices,  $\beta$  strands, and loops are depicted as ribbons, arrows, and threads, respectively. The partner molecules of Ets1 in the Ets1–Runx1–CBF $\beta$ –DNA complex are represented by magenta (Runx1)/cyan (CBF $\beta$ ) and those in the Ets1–Pax5–DNA complex in blue (Pax5). The DNA molecule is depicted as gray sticks. The NMR structure of free Ets1 is shown instead of the crystal structure because free Ets1 takes a pseudodimeric form with domain swapping of each HI-1 in the crystal. This free Ets1 structure corresponds to the T conformer (see Discussion). (e–h) Magnified views of the Ets1 structures in (a–d). The side chains of residues involved in the Ets1 hydrophobic core are shown in space-filling representations. (i–l) Schematic representations of regions of the Ets1 structures in (e–h). Residues involved in the hydrophobic core are shown as light-orange ovals. The hydrogen bonds are represented as black broken lines. (m) A superimposed view of the DNA structures in Ets1-containing DNA complexes. The structures were superimposed using the least-squares method to fit the amino acid region spanning residues 330–430 in each Ets1. Within the DNA molecules, tubes indicate the DNA backbones, transparent sticks indicate all heavy atoms, and their helical axes are depicted as thick lines in the Ets1–Runx1–CBF $\beta$ –DNA (orange), (Ets1)<sub>2</sub>–DNA (yellow), and Ets1–Pax5–DNA (green) complexes. For simplicity, only one strand of the DNA molecule is shown. The sugar C4' atom of the guanine at position 11 (see Fig. 2a for base pair positions) in the Ets1–Runx1–CBF $\beta$ –DNA complex is shown as a space-filling sphere. The Ets1 molecules in the Ets1–Runx1–CBF $\beta$ –DNA and Ets1–Pax5–DNA complexes are shown in a superimposed view and colored orange and green, respectively. The side chain of Pro334 in Ets1 in the Ets1–Runx1–CBF $\beta$ –DNA complex is shown as sticks with space-filling spheres. The inset shows a close-up view of the indicated region.

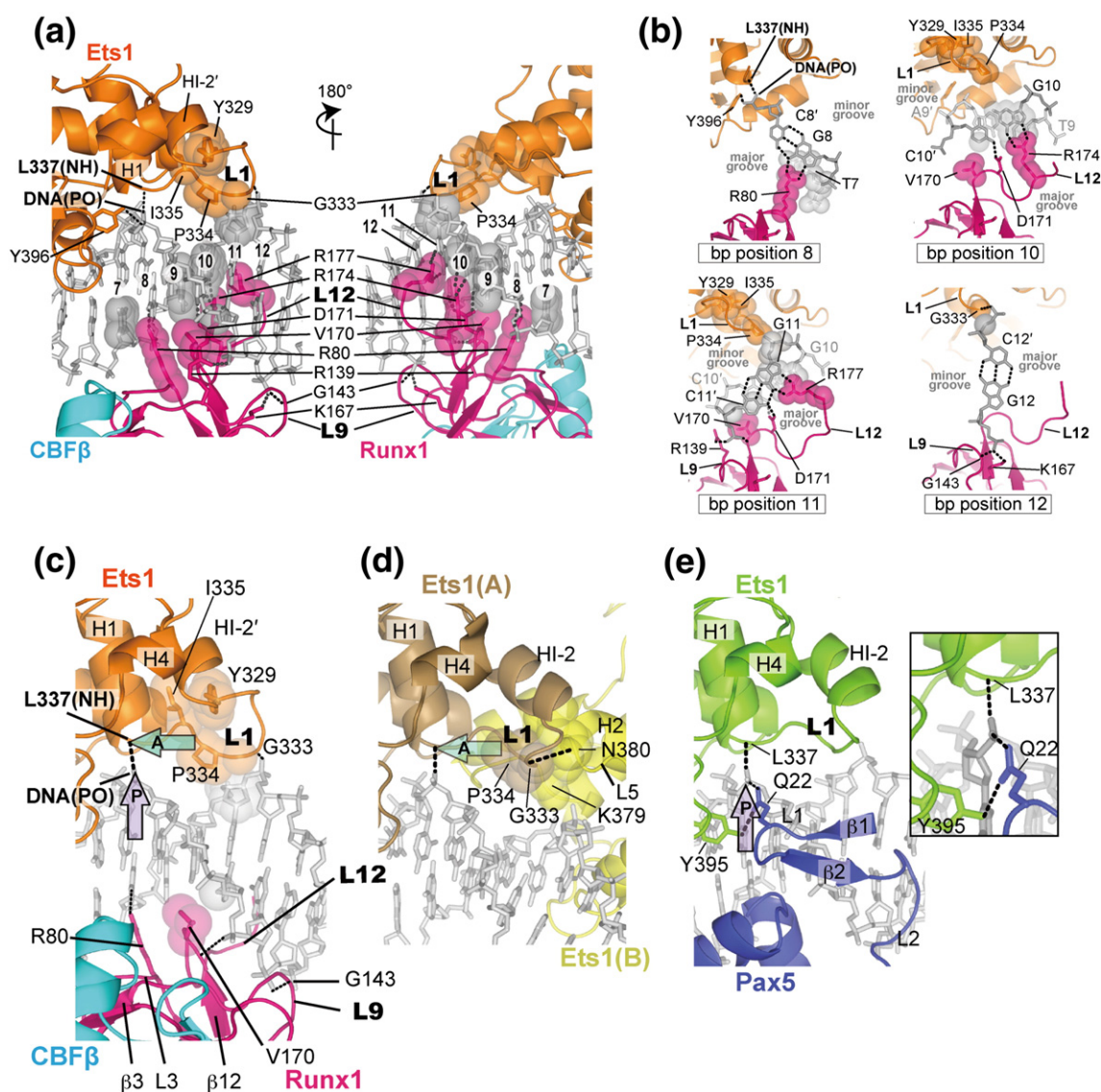


**Fig. 2.** Interaction network among Ets1, DNA, and Runx1 within the Ets1–Runx1–CBF $\beta$ –DNA complex and its comparison with other Ets1-containing complexes. (a and b) Front and back views of Ets1–DNA–Runx1 interactions (a) and cross-sections at the indicated positions (b) (base pair positions are numbered according to Figs. S1b and S5). The side chains of Tyr329, Pro334, and Ile335 in Ets1 and the side chains of Arg80, Val170, Asp171, Arg174, and Arg177 in Runx1 are shown as sticks with space-filling spheres. The C $^{\alpha}$  atom of Gly333 in Ets1 is depicted as a space-filling sphere, and the side chains of Arg139 and Lys167 in Runx1 are shown as sticks. The numbers in circles on the DNA indicate the base pair positions. The thymine and guanine bases at positions 7, 9, and 10; C5 of cytosine at position 10; all heavy sugar atoms of guanine and C2' of cytosine at position 11; and C5' of cytosine at position 12 are shown as space-filling representations. Hydrogen bonds are shown as dark-gray dotted lines. (c–e) Detailed views of Ets1-containing DNA complexes with indications of the structural stabilization pathways. The A and P pathways (see the text) are depicted as blue-green and light-purple arrows, respectively. The inset in (e) shows a close-up view of the hydrogen bond between the side chain of Gln22 in Pax5 and a DNA phosphate in the Ets1–Pax5–DNA complex. Colors are as in Fig. 1.

the behavior of phosphorylated Ets1 in the presence of partner TFs on target enhancers remains unclear. To investigate this further, we used EMSAs to assess the binding of unphosphorylated and phosphorylated Ets1 in the presence or absence of Runx1 to the *TCRA* enhancer, Pax5 to the *mb-1* enhancer, and dimeric Ets1 to the *stromelysin-1* enhancer.

In the absence of partner TFs, phosphorylation of Ets1 almost completely abolished binding to all three enhancers [equilibrium association constant ( $K_A$ ) <  $1 \times 10^6 \text{ M}^{-1}$ ] (Fig. 3c–e, Fig. S9b and d, and Tables S4 and S6). Conversely, in the presence of Runx1, phosphorylated Ets1 was capable of binding the *TCRA* enhancer with relatively high

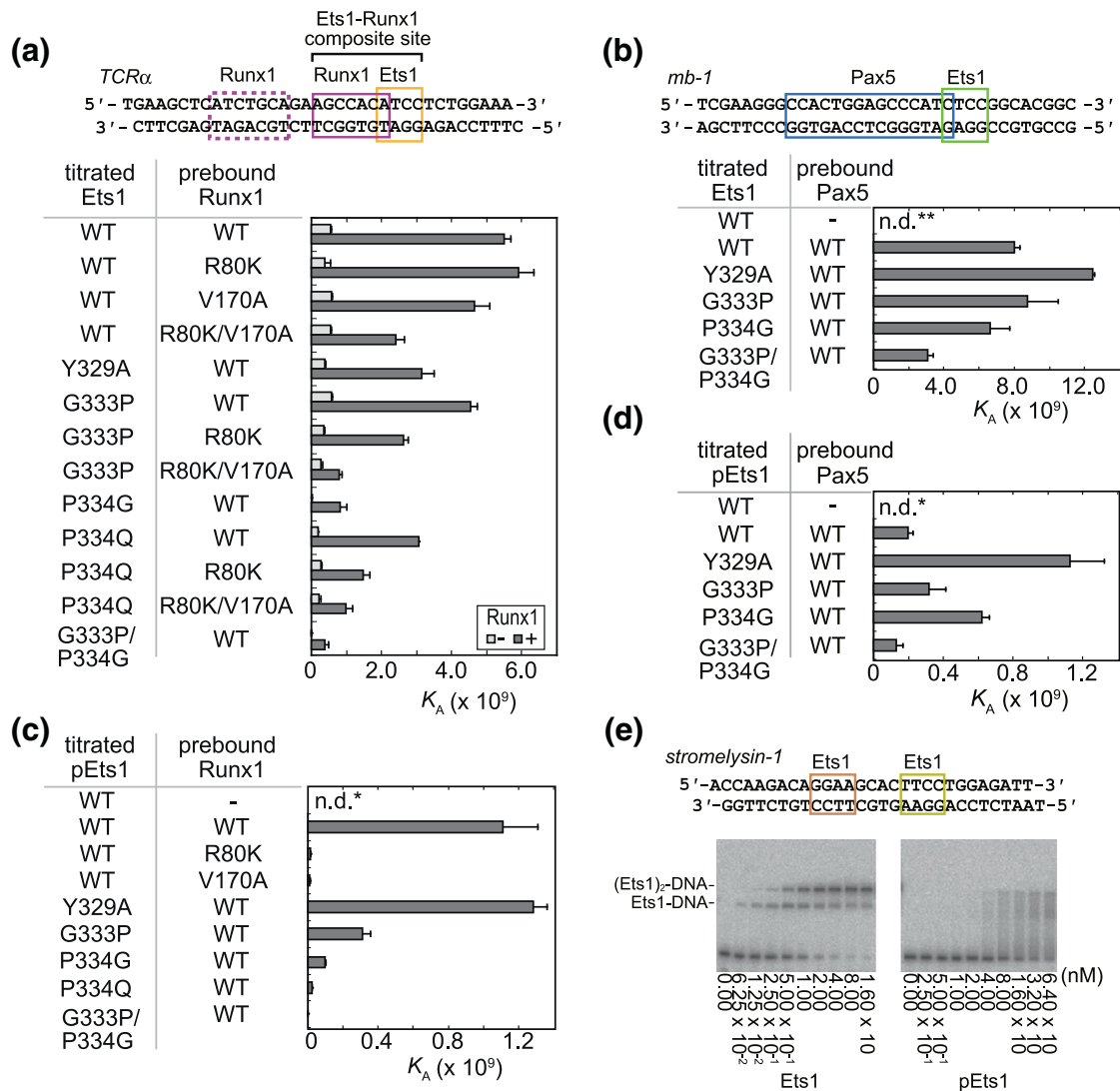


**Fig. 3.** Mutational characterization of the cooperative DNA binding of unphosphorylated or phosphorylated Ets1 and its partner TFs. (a–d)  $K_A$  values for the DNA binding of unphosphorylated (a and b) and phosphorylated (c and d) Ets1 (276–441) in the presence and absence of Runx1 (60–263) on the *TCRα* enhancer (a and c) or of Pax5 (1–149) on the *mb-1* enhancer (b and d). The sequences of the DNA fragments from the *TCRα* and *mb-1* enhancers are shown in (a) and (b). Another Runx1 binding site adjacent to the Ets1–Runx1 composite site in the native *TCRα* enhancer is boxed in magenta broken lines. This site was disrupted by mutagenesis because it is not involved in the cooperative binding of Ets1 and Runx1. Data are presented as the mean  $\pm$  SEM (standard error of the mean) ( $n = 3$ ). WT, wild type; pEts1, phosphorylated Ets1; n.s., data not shown because the DNA binding affinity was too low ( $K_A < 1\text{--}5 \times 10^9 \text{ M}^{-1}$ ) (n.s.\*) or because of cooperative binding of multiple Ets1 molecules to the *mb-1* enhancer (n.s.\*\*). (e) EMSAs showing the DNA binding of unphosphorylated and phosphorylated Ets1 to the *stromelysin-1* enhancer. The sequence of the DNA fragment and the concentrations of Ets1 used in the titration are indicated.

affinity ( $K_A = 1.1 \times 10^9 \text{ M}^{-1}$ ) (Fig. 3c, Fig. S9b compared with a, and Table S4). In contrast, phosphorylated Ets1 exhibited a 40-fold reduction in binding at the *mb-1* enhancer, even in the presence of its partner TF, Pax5 (Fig. 3d, Figs. S7 and 9d compared with 9c, and Table S6). Similarly, EMSA analysis revealed that phosphorylation of Ets1 almost completely abolished DNA binding to the *stromelysin-1* enhancer (Fig. 3e). These findings

indicate that binding of Runx1 to the *TCRα* enhancer abrogates phosphorylation-induced inhibition of Ets1 binding to DNA. In contrast, binding of Pax5 to the *mb-1* enhancer or of dimerized Ets1 to the *stromelysin-1* enhancer did not.

Importantly, in the case of the *TCRα* enhancer, impairment of either A or P pathway by the introduction of a single mutation in Ets1 (G333P or P334G) or Runx1 (V170A or R80K) (Fig. 2c and Fig. S6a)

abrogated cooperative DNA binding of phosphorylated Ets1 with Runx1 (Fig. 3c, Fig. S7, and Table S4). These data highlight the stability of the Ets1 complex, which is provided by the redundancy of the A and P pathways. Such redundancy is critical for Ets1-containing complexes to resist the inhibitory effect of Ets1 phosphorylation on DNA binding.

### The effect of Ets1 phosphorylation on target gene transactivation

We next used luciferase reporter assays to examine the effect of Ets1 phosphorylation on transactivation of Ets1 target genes. HeLa or HEK293T cells were co-transfected with expression plasmids encoding Ets1 and Runx1–CBF $\beta$  or Pax5, with or without a plasmid encoding a constitutively active CaMKII (T287D) mutant [24,42], in addition to reporter plasmids containing the *TCR $\alpha$* , *mb-1*, or *stromelysin-1* enhancers (Fig. 4a–c). Expression plasmids encoding an Ets1 splice variant lacking exon VII (p42) or a S251A/S257A/S282A/S285A mutant (4A), both of which are incapable of being phosphorylated, were also used as controls (Figs. S1a and 10a). Cooperative transactivation of the *TCR $\alpha$*  enhancer by wild-type Ets1 and Runx1 was fully preserved in the presence of CaMKII (T287D), and similar results were obtained with the p42 or 4A mutant forms of Ets1 (Fig. 4a). In contrast, co-expression of CaMKII (T287D) significantly reduced cooperative transactivation of the *mb-1* enhancer by wild-type Ets1 and Pax5 and of the *stromelysin-1* enhancer by wild-type Ets1. However, cooperative transactivation was fully preserved when the p42 or 4A mutant forms of Ets1 were expressed instead of wild-type Ets1 (Fig. 4b and c). Thus, the inhibitory effect of Ets1 phosphorylation on transactivation is specifically countered by Runx1 on the *TCR $\alpha$*  enhancer.

We also examined the effect of Ets1 and Runx1 mutations on the transactivation of Ets1 target genes. Note that the tested mutations would impair either the A or P pathways in the allosteric network mediating binding cooperativity. Consistent with the EMSA data, cooperative transactivation by phosphorylated Ets1 and Runx1 was reduced by mutation of Ets1 (G333P or P334G) or Runx1 (V170A) affecting the A pathway or by mutation of Runx1 (R80K) affecting the P pathway (Fig. 4d).

### Target gene selection through phosphorylation of Ets1 in cells

To investigate the effect of Ets1 phosphorylation on Ets1 binding to *TCR $\alpha/\beta$*  and *mb-1* enhancers and to other reported Ets1 target genes [43] in cells, we performed chromatin immunoprecipitation (ChIP) analyses in the human Jurkat T cell line and the mouse WEHI-231 B cell line, following induction of Ets1 phosphorylation with ionomycin (a Ca<sup>2+</sup>

ionophore) and phosphatase inhibitors (Fig. S10b). In the absence of ionomycin treatment, enrichment of Ets1 was observed at all tested Ets1 target genes, compared with a negative control region (the 3' region of the *albumin* gene), in both Jurkat and WEHI-231 cells (Fig. 5a and b). Following treatment with ionomycin and phosphatase inhibitors, DNA-bound Ets1 tended to dissociate from a number of Ets1 target genes, including *mb-1* in WEHI-231 cells (Fig. 5a and b). However, Ets1 binding to the *TCR $\alpha/\beta$*  gene was almost completely retained in Jurkat cells, even after treatment (Fig. 5a). Notably, although enrichment of Ets1 on the *TCR $\alpha$*  enhancer was also detected in WEHI-231 cells, it was reduced by treatment with ionomycin and phosphatase inhibitors (Fig. 5b).

We next investigated the expression of several Ets1 target genes following Ets1 phosphorylation. The resultant data were essentially consistent with the ChIP-qPCR (quantitative PCR) data (Fig. S11). These observations suggest that phosphorylation of Ets1 alters its target gene repertoire, depending upon the context of the enhancer and the partner TFs present (Fig. 5c).

## Discussion

Allostery is the process by which biological macromolecules, such as proteins, transmit information about the conformational state induced by the binding of an effector at one site to a different site, enabling the effector to regulate molecular function from a distance. Previous structural studies for TF–DNA complexes suggest that the allosteric nature of DNA plays a key role in the process of assembling TF–DNA complexes [44,45]. In this study, we focused on the stabilization of TF assembly, as well as its regulation by phosphorylation of a component via cell signaling, in the context of protein and DNA allostery.

Widely accepted theories of intermolecular interactions include the conformational selection model and the induced-fit model. In the conformational selection model, proteins with intrinsically dynamic natures achieve molecular recognition by selecting partners with favorable conformations, from a variety of conformations in a pre-existing conformational repertoire [46,47]. This model is considered to function predominantly at low ligand concentrations [48]. Based on this model, it is assumed that effector binding to an allosteric molecule modulates its conformationally fluctuating space. Thus, the effector changes the target's conformer distribution, which affects the dynamic state of a distant critical site to regulate molecular function.

If the “conformational distribution change” model [46,47] for allostery is applied to the assembly of TF–DNA complexes involving Ets1, the equilibrium relation for Ets1 conformers in the various DNA-

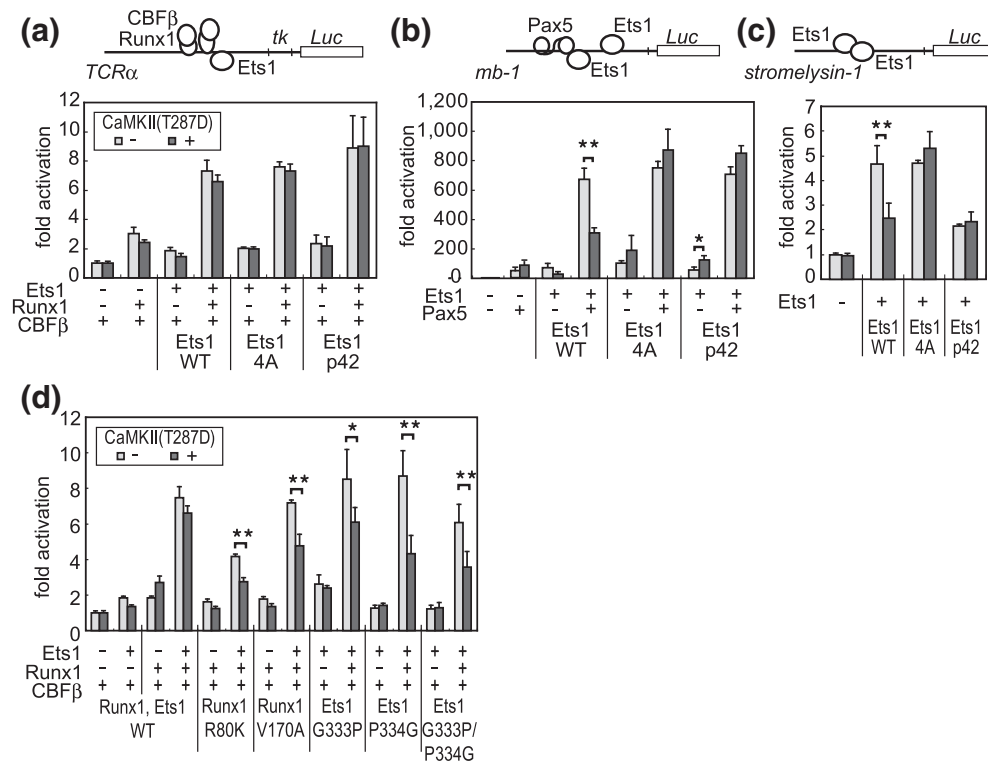


**Fig. 4.** Cooperative transactivation activities of unphosphorylated and phosphorylated Ets1 with other TFs on three target gene enhancers. (a–d) Luciferase reporter assays for Ets1 target genes showing transactivation of the *TCRα* enhancer *thymidine kinase* (*tk*) promoter (a and d), the *mb-1* enhancer (b), and the *stromelysin-1* enhancer (c) in the presence (dark gray) and absence (light gray) of constitutively active CaMKII (T287D). Schematic representations of the reporter constructs with the TFs bound are shown on the top (a–c). In (d), the indicated mutant forms of full-length Ets1 and Runx1 were used. In all cases, data were calculated as fold activation relative to the reporter-only control and are presented as means  $\pm$  SD ( $n = 3$ ). WT, wild type; \* $P < 0.05$  and \*\* $P < 0.01$ .

complexed states is schematically illustrated in Fig. 6a. In this model, free Ets1 fluctuates between a major conformer *T* and two minor conformers, *R1* and *R2*. The inhibitory module is organized in the *T* conformer, partly disorganized with disordered HI-1 in the *R1* conformer and extensively disorganized in the *R2* conformer. This conformational equilibrium among *T*, *R1*, and *R2* becomes shifted toward the *T* state upon Ets1 phosphorylation.

In the presence of partner TFs, the *R1* and *R2* conformers of Ets1 preferentially recognize the *mb-1* enhancer bound to Pax5 and the *TCRα* enhancer bound to Runx1–CBFβ, respectively. The Ets1-bound *stromelysin-1* enhancer is also preferentially recognized by the *R1* conformer. Thus, DNA and TFs, including Ets1, are considered to behave as mutually allosteric molecules and effectors (Fig. 6b).

In this study, we demonstrate that Ets1 changes its target gene repertoire in response to phosphorylation. We performed detailed structural and molecular analyses to investigate the molecular mechanisms underlying this phosphorylation-dependent target gene selection, from the viewpoint of cooperative Ets1 binding with its partner TFs on three Ets1 target

enhancers. When bound with Runx1 on the *TCRα* enhancer, the *R2* conformer of Ets1 forms an allosterically stabilized complex with a unique conformational transition mediated by the enhancer DNA. This is achieved via multiple stabilization pathways directing a hydrogen bond between a protein main-chain amide and a DNA backbone phosphate (Figs. 2c and 6b), which becomes insensitive to the inhibitory effect of Ets1 phosphorylation on Ets1–DNA binding. In contrast, on the Pax5-bound *mb-1* enhancer or the *stromelysin-1* enhancer, the *R1* conformer of Ets1 and its partner TF form a DNA complex with a less extensive interaction network mediated via a single pathway stabilizing the hydrogen bond, which is sensitive to the inhibitory effect of phosphorylation (Fig. 2d and e).

It is noteworthy that the stability of a common and characteristic hydrogen bond between a protein main-chain amide and a DNA backbone phosphate appears to be critical for allosteric regulation of a variety of other TF–DNA complexes [2,3,38]. This suggests that the mechanism for target gene-specific regulation of Ets1 activity is likely applicable to regulatory systems involving other TF assemblies on

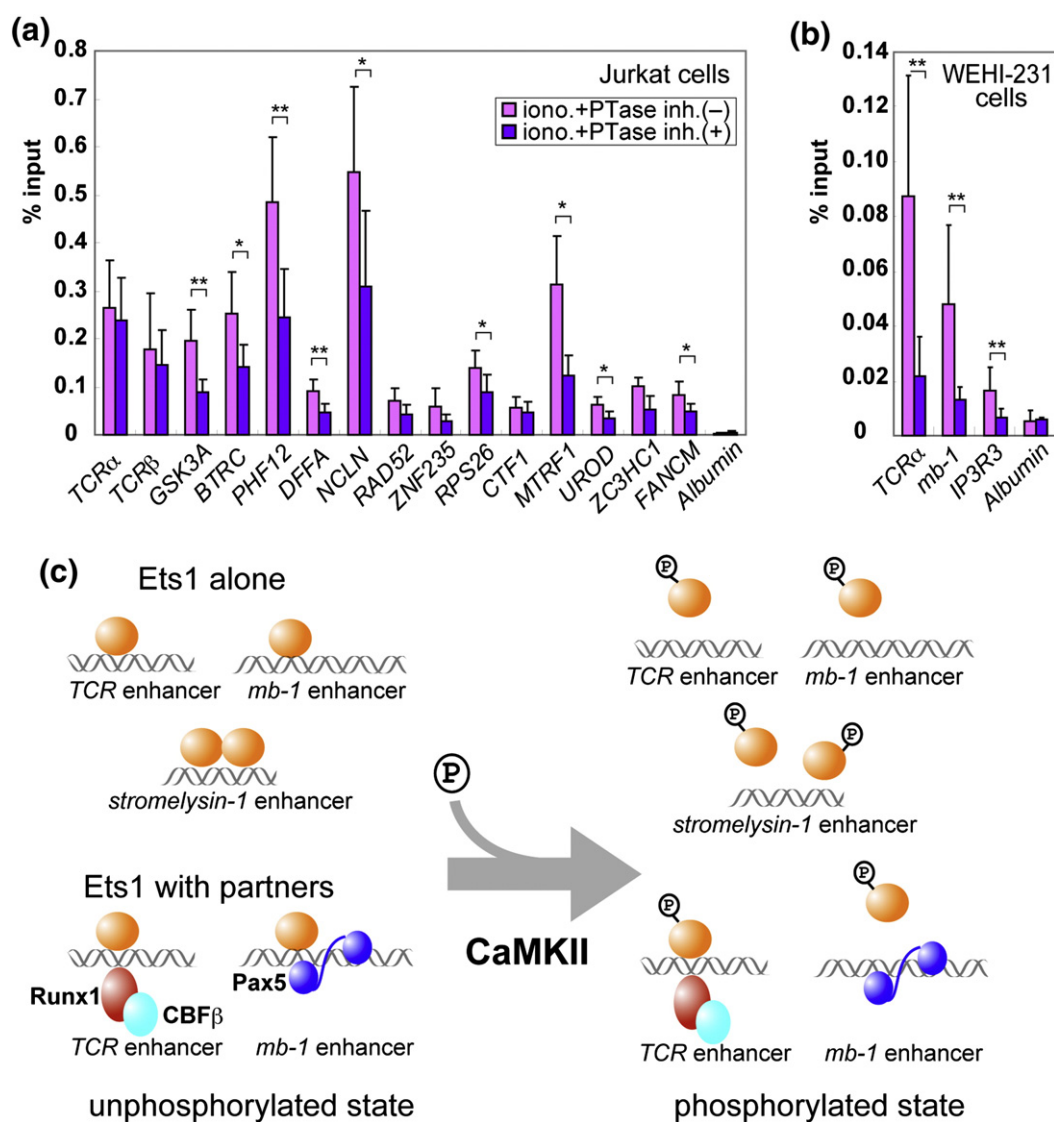


**Fig. 5.** ChIP-qPCR analyses of the binding of unphosphorylated and phosphorylated Ets1 to target enhancers in cells. (a and b) ChIP enrichment values for Ets1 on target enhancers in Jurkat (a) and WEHI-231 (b) cells, in the presence (blue) and absence (purple) of ionomycin and phosphatase inhibitors (iono. + PTase inh.). ChIP data are presented as percentages of input (% input)  $\pm$  SD ( $n = 3$ ). \* $P < 0.05$  and \*\* $P < 0.01$ . (c) Diagram of the changes in the Ets1 distribution on target genes induced by CaMKII-catalyzed Ets1 phosphorylation.

their respective target enhancers. Taken together, our study demonstrates that precise transcriptional modulation may be attained by chemical modification of TFs, where allostery involving DNA may play an important role.

Recently, a direct interaction model between Ets1 and Runx1 on the *TCRα* enhancer was proposed by Shrivastava *et al.* [49]. In their model, a C-terminal region (190–212) of the Runt domain (50–177) interacts with Ets1 on the DNA through a missing loop (178–189) of Runx1, based on their crystal structures. The position of the N-terminus of the Ets1-interacting region of Runx1 (Gly190), however,

appears spatially too distant from that of the C-terminus of Runt domain (Arg177) to be connected through a 13-mer polypeptide corresponding to the amino acid region 178–189 within a complex. This raises a question whether the interaction of Runx1 with Ets1 in their structure would be inter-complex interaction in the crystal. Because our EMSA data suggested that the C-terminal region of the Runt domain enhances the cooperativity with Ets1 on the *TCRα* enhancer (Fig. S2), further structural and functional study will be required to evaluate the integrity of their direct interaction model for the cooperativity between Ets1 and Runx1.

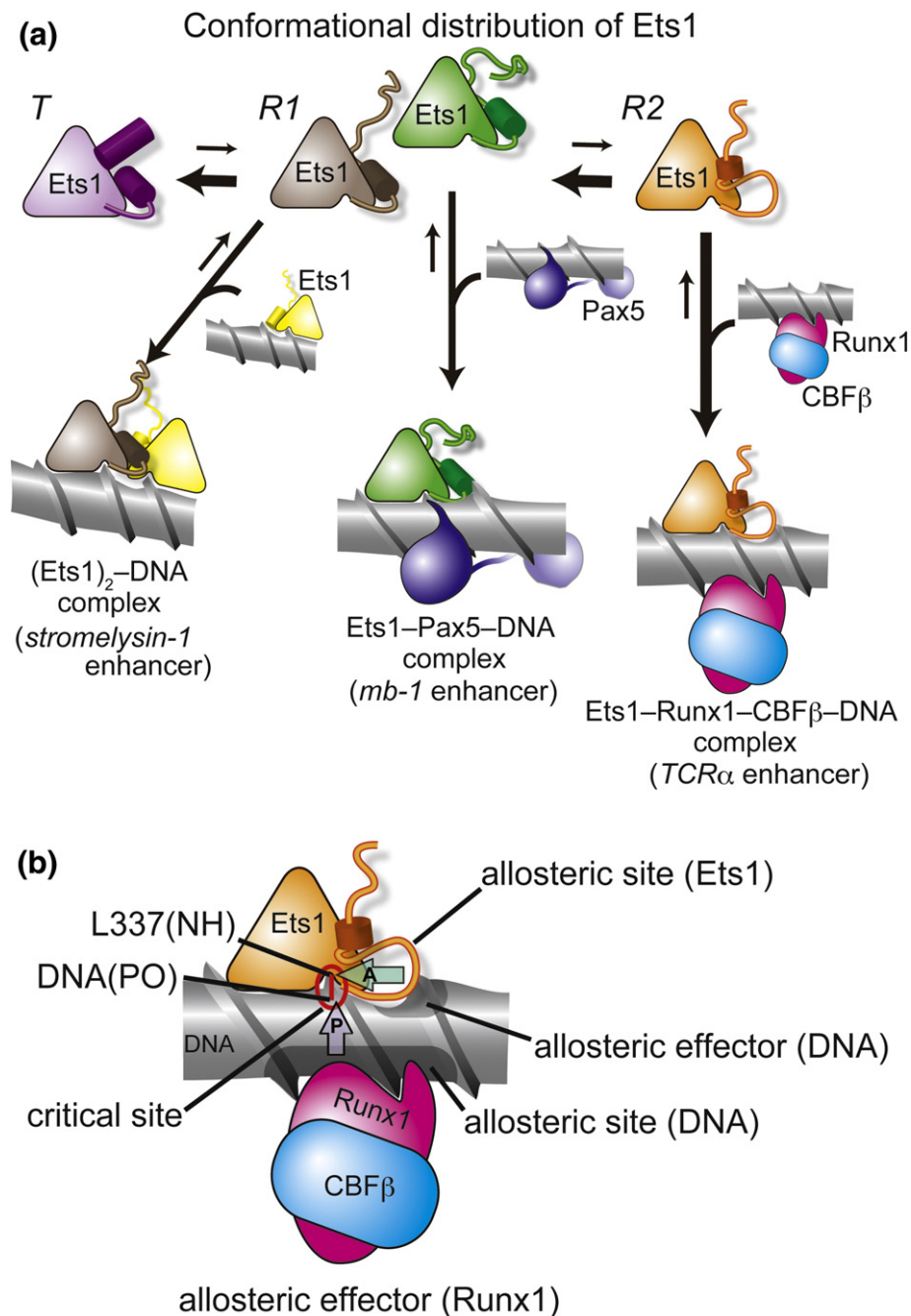


**Fig. 6.** Conformational selection model for Ets1 by a partner within TF–DNA complexes, as well as roles of Ets1, Runx1, and DNA in the allosteric regulation of their assembly. (a) Three distinct Ets1 conformations observed in structural analyses are schematically represented with *T*, *R1*, and *R2* annotations. The Ets1 molecule is colored as for Fig. 1. The Ets domain is depicted as a triangle-like shape, and a helix and a loop within the N-terminal extension of the Ets domain are shown as a cylinder and a thread. DNA is shown as a gray bamboo-like shape in which the nodes represent the sugar-phosphate ridges. Runx1 and CBFβ are depicted as ovals, and Pax5 is depicted as two ovals with a thread linker, each colored as in Fig. 1. (b) Roles of Ets1, Runx1, and DNA in the allosteric regulation of their assembly. Allosteric effectors and their binding sites are indicated. In the DNA, the allosteric effector Runx1 binding site (the allosteric site) and the allosteric effector site for Ets1 are shaded dark gray. The red-circled position of the hydrogen bond between L337(NH) and DNA(PO) corresponds to the critical site for the Ets1–DNA binding regulation. Illustrations of the molecules and the arrow marks are the same as for (a) and Fig. 2c, respectively.

## Materials and Methods

### Protein expression, purification, crystallization, X-ray diffraction, and structure determination

Sample preparation, crystallization, and cryoprotection of crystals were performed as previously described (Shiina *et al.*). Diffraction data were collected on beamline BL41XU at SPring-8 (Harima, Japan) and on beamlines BL17A and NW12A at the Photon Factory at KEK (Tsukuba, Japan). Detailed protocols for structure determination are described in Supplementary Methods.

### Preparation for phosphorylated fragments of Ets1

Ets1 fragments (276–441) phosphorylated on Ser282 and Ser285 were prepared as described previously [41]. Briefly, recombinant CaMKII was purified from a baculovirus expression system, which was kindly provided by Dr. Thomas Soderling (Oregon Health Sciences University). Phosphorylation reaction was performed by incubating Ets1 fragments (100  $\mu$ M at final concentration) for 3 h at 30 °C in buffer containing 50 mM Hepes-Na (pH 7.5), 10 mM magnesium acetate, 0.5 mM  $\text{CaCl}_2$ , 1 mM ATP, 2 mM DTT, 1  $\mu$ M calmodulin, and 0.2  $\mu$ M CaMKII.

### Electrophoretic mobility shift assays

Equilibrium constants for protein–DNA interactions were determined using quantitative EMSAs. DNA fragments were purified using polyacrylamide gel electrophoresis and end-labeled with [ $\gamma$ - $^{32}\text{P}$ ]ATP. DNA binding reactions were performed in buffer containing 20 mM Tris–HCl (pH 7.2), 150 mM KCl, 1 mg/mL bovine serum albumin, 10 mM DTT, 50  $\mu$ g/ $\mu$ M poly(dI-dC), 0.005% Tween 20, and 2.5% Ficoll for 20 min at 4 °C. Increasing concentrations of protein were incubated with DNA (<1 pM) in reaction mixtures containing free DNA or pre-formed protein–DNA complexes. Pre-formed protein–DNA complexes were prepared by mixing DNA with an appropriate amount of protein, to produce target complexes including >90% of the total DNA band. Complexes were resolved on 8% polyacrylamide gels following electrophoresis at 150 V for 40 min at 4 °C. Autoradiograms were developed using a Bio-Image analyzer BAS 2500 (Fujifilm), and the density of each band was quantified using ImageGauge v. 4.23 software (Fujifilm). Equilibrium dissociation constants ( $K_D$ ) were determined by plotting the proportion of protein-bound DNA in the total DNA ( $[\text{Protein–DNA (PD)}]/[\text{Total DNA (Dt)}]$ ) against the protein concentration ( $[P]$ ) as previously described [29].  $K_D$  values and standard errors were calculated using nonlinear least-squares fitting of the average values from three data points to  $[\text{PD}]/[\text{Dt}] = 1/(1 + (K_D/[P]))$  using the gnuplot software package. To evaluate cooperative DNA binding of proteins A and B, we plotted a super-shifted band ( $P_A P_B D$ ) obtained by titration of protein A against the protein B–DNA complex ( $P_B D$ ) against the protein A concentration  $[P_A]$ . Data were then fitted to the following model:  $[P_A P_B D]/[\text{Dt}] = 1/(1 + (K_D/[P_A]))$ , where  $[\text{Dt}] = [P_B D] + [P_A P_B D]$ , ignoring free DNA  $[D]$ . DNA binding affinities are presented as equilibrium association constant ( $K_A$ ) values, the inverse of the  $K_D$  values.

### Luciferase reporter assays

Luciferase reporter constructs were prepared by subcloning the minimal human *TCR $\alpha$*  enhancer (position 12–109) [16], the human *mb-1* enhancer (position –525/+26) [50], and the human *stromelysin-1* enhancer (position –478/+4) [51], upstream of the *luciferase* gene in the pGL3 basic vector (Promega). HeLa and HEK293T cells were cultured in Dulbecco's modified Eagle's medium supplemented with 10% fetal calf serum. The cells were transiently co-transfected with the appropriate reporter plasmid and expression plasmids pCG-Ets1, pCAGGS-Runx1, pEF-BOS-CBF $\beta$ , or pcDNA3.1-Pax5, encoding full-length human Ets1 (1–441), mouse Runx1 isoform 1 (1–451), mouse CBF $\beta$  (1–187), or mouse Pax5 (1–391), respectively, in the presence or absence of pSRalpha.BKS-CaMKII(T287D) [24,42], which encodes a constitutively active human CaMKII (T287D) mutant. DNA transfection was performed using PolyFect (Qiagen) or Lipofectamine 2000 (Invitrogen) in accordance with the manufacturer's instructions. Luciferase activity was assayed using the dual-luciferase reporter assay system (Promega) with a Berthold-designed luminometer (Centro LB960) according to the manufacturer's instructions.

Data are expressed as fold activation relative to the reporter-only control and represent the mean  $\pm$  SD ( $n = 4$ ). Statistical significance was evaluated using an unpaired, two-tailed *t* test.

### ChIP assay

Jurkat and WEHI-231 cells were purchased from the American Type Culture Collection and cultured in accordance with the supplier's instructions. For induction of Ets1 phosphorylation, cells were treated with ionomycin (1  $\mu$ g/mL) and a cocktail of phosphatase inhibitors including sodium orthovanadate (1 mM),  $\beta$ -glycerophosphate (10 mM), and NaF (10 mM) for 30 min (Jurkat cells) or 15 min (WEHI-231 cells) at 37 °C under a 5%  $\text{CO}_2$  atmosphere. The phosphorylation reaction was terminated by formaldehyde cross-linking for 15 min at room temperature (25 °C).

ChIP assays were performed as previously described [43]. Briefly, Dynabeads were conjugated with anti-Ets1 rabbit immunoglobulin G (sc-350; Santa Cruz Biotechnology, Inc.) or control rabbit immunoglobulin G (Santa Cruz Biotechnology, Inc.). Nuclei were isolated from  $1.0 \times 10^7$  cells and chromatin was sonicated for 30 min at 4 °C in 250  $\mu$ L of nuclear lysis buffer [50 mM Tris–HCl (pH 7.9), 10 mM ethylenediaminetetraacetic acid (EDTA), 1% SDS, and 1 $\times$  protease inhibitor cocktail (Roche)] using a Bioruptor (Cosmo Bio). Chromatin extracts were incubated with Dynabeads for 6 h at 4 °C on a rotating wheel. Dynabeads were then washed with immunoprecipitation wash buffer [20 mM Tris–HCl (pH 7.9), 0.25% NP-40, 0.005% SDS, 2 mM EDTA, and 250 mM NaCl] (3 $\times$ , 5 min) at 4 °C, followed by TE buffer [10 mM Tris–HCl (pH 8.0) and 1 mM EDTA] containing 50 mM NaCl (1 $\times$ , 5 min) at 4 °C. The beads were then resuspended in 100  $\mu$ L TE buffer containing RNase (100  $\mu$ g/mL) and incubated for 30 min at 37 °C. SDS (1% w/v) and proteinase K (100  $\mu$ g/mL) were subsequently added to the bead slurry and samples were incubated for 3 h at 55 °C and subsequently for 8 h at 65 °C. The immunoprecipitated DNA was extracted using

phenol/chloroform and purified using a PCR purification kit (Qiagen).

### Real-time PCR

Real-time PCR was performed using SYBR Premix DimerEraser (TaKaRa) with a LightCycler 480 Real-Time PCR System (Roche). PCR primers targeting human *Ets1* binding sites, the 3' region of the human *albumin* gene (as a negative control), and the mouse *IP<sub>3</sub>R3* enhancer were previously described [43,52]. Primer sequences for the mouse *mb-1* enhancer, mouse *TCR $\alpha$*  enhancer, and the 3' region of the mouse *albumin* gene were designed using Primer3Plus and are as follows: *mb-1* forward 5'-CACC TCTCAGGGGAATTGTG-3', reverse 5'-ACCAGATCCC TACCCCAAAC-3'; *TCR $\alpha$*  forward 5'-CCAGAAGTAGAA CAGGAAATGGA-3', reverse 5'-TTTCCAGAGGATGTGG CTTC-3'; *albumin* 3' ORF forward 5'-TACAGCGGAGCA ACTGAAGA-3', reverse 5'-GACCACGTGCACAG AAAATG-3'. The ChIP data are presented as percentages of input (% input) and represent the mean of three independent experiments  $\pm$  SD. Statistical significance was evaluated using an unpaired, two-tailed *t* test.

### Accession codes

Atomic coordinates and structure factors for the reported structures have been deposited with the Protein Data Bank under accession codes **3WTS** (Ets1–Runx1–CBF $\beta$ –DNA complex), **3WTT** (phosphorylated Ets1–Runx1–CBF $\beta$ –DNA complex), **3WTU** [Ets1–Runx1(V170A)–CBF $\beta$ –DNA complex], **3WTX** [Ets1(Y329A)–Runx1–CBF $\beta$ –DNA complex], and **3WTY** [Ets1(G333P)–Runx1–CBF $\beta$ –DNA complex].

### Acknowledgments

We thank Shunsuke Ishii, Akinori Sarai, and Akio Yamashita for their helpful discussions. The Pax5 expression vector was a kind gift from Kazuhiko Igarashi. The expression vectors for CaMKII and its mutant were kindly provided by Howard Schulman. We also thank Yukimi Uchiyama and Ayako Shirai for support with the manuscript preparation and Naomichi Matsumoto for generous technical support. This work was supported, in part, by a Grant-in-Aid for Scientific Research on Priority Areas, a Grant-in-Aid for Scientific Research on Innovative Areas "Transcription Cycle" 24118005, and the Special Coordination Funds for Promoting Science and Technology "Creation of Innovation Centers for Advanced Interdisciplinary Research Areas" from the Ministry of Education, Culture, Sports, Science and Technology, Japan, to K.O.

**Author Contributions:** M.Shiina, T.I.-B., and M.Shimamura prepared the crystals; M.Shiina, K.H., and M.Y. solved the structures; T.I.-B., M.Shimamura,

A.U., S.B., and K.S. prepared samples and performed biochemical experiments; M.Shiina and A.U. analyzed the data; and M.Shiina and K.O. wrote the manuscript and conceived or designed the experiments.

**Competing Financial Interests:** The authors declare no competing financial interests.

### Appendix A. Supplementary data

Supplementary data to this article can be found online at <http://dx.doi.org/10.1016/j.jmb.2014.07.020>.

Received 25 April 2014;

Received in revised form 27 June 2014;

Accepted 17 July 2014

Available online 30 July 2014

#### Keywords:

allosteric regulation;

Ets1;

phosphorylation;

Runx1;

TCR $\alpha$  enhancer

†T.I.-B. and M.S. contributed equally to this work.

#### Abbreviations used:

TF, transcription factor; EMSA, electrophoretic mobility shift assay; ChIP, chromatin immunoprecipitation; EDTA, ethylenediaminetetraacetic acid.

### References

- [1] Thanos D, Maniatis T. Virus induction of human IFN $\beta$  gene expression requires the assembly of an enhanceosome. *Cell* 1995;83:1091–100.
- [2] Tahirov TH, Sato K, Ichikawa-Iwata E, Sasaki M, Inoue-Bungo T, Shiina M, et al. Mechanism of c-Myb-C/EBP $\beta$  cooperation from separated sites on a promoter. *Cell* 2002;108:57–70.
- [3] Ogata K, Sato K, Tahirov TH. Eukaryotic transcriptional regulatory complexes: cooperativity from near and afar. *Curr Opin Struct Biol* 2003;13:40–8.
- [4] Okamura H, Aramburu J, Garcia-Rodriguez C, Viola JP, Raghavan A, Tahiliani M, et al. Concerted dephosphorylation of the transcription factor NFAT1 induces a conformational switch that regulates transcriptional activity. *Mol Cell* 2000; 6:539–50.
- [5] Qin BY, Lam SS, Correia JJ, Lin K. Smad3 allostery links TGF- $\beta$  receptor kinase activation to transcriptional control. *Genes Dev* 2002;16:1950–63.
- [6] Becker S, Groner B, Müller CW. Three-dimensional structure of the Stat3 $\beta$  homodimer bound to DNA. *Nature* 1998; 394:145–51.
- [7] Chen X, Vinkemeier U, Zhao Y, Jeruzalmi D, Darnell JE, Kuriyan J. Crystal structure of a tyrosine phosphorylated STAT-1 dimer bound to DNA. *Cell* 1998;93:827–39.
- [8] Radhakrishnan I, Perez-Alvarado GC, Parker D, Dyson HJ, Montminy MR, Wright PE. Solution structure of the KIX

- domain of CBP bound to the transactivation domain of CREB: a model for activator:coactivator interactions. *Cell* 1997;91:741–52.
- [9] Parker D, Jhala US, Radhakrishnan I, Yaffe MB, Reyes C, Shulman AI, et al. Analysis of an activator:coactivator complex reveals an essential role for secondary structure in transcriptional activation. *Mol Cell* 1998;2:353–9.
- [10] Lee GM, Donaldson LW, Pufall MA, Kang HS, Pot I, Graves BJ, et al. The structural and dynamic basis of Ets-1 DNA binding autoinhibition. *J Biol Chem* 2005;280:7088–99.
- [11] Brent MM, Anand R, Marmorstein R. Structural basis for DNA recognition by FoxO1 and its regulation by posttranslational modification. *Structure* 2008;16:1407–16.
- [12] Lee GM, Pufall MA, Meeker CA, Kang HS, Graves BJ, McIntosh LP. The affinity of Ets-1 for DNA is modulated by phosphorylation through transient interactions of an unstructured region. *J Mol Biol* 2008;382:1014–30.
- [13] Dittmer J. The biology of the Ets1 proto-oncogene. *Mol Cancer* 2003;2:29.
- [14] Ogawa E, Inuzuka M, Maruyama M, Satake M, Naito-Fujimoto M, Ito Y, et al. Molecular cloning and characterization of PEBP2 $\beta$ , the heterodimeric partner of a novel *Drosophila* runt-related DNA binding protein PEBP2 $\alpha$ . *Virology* 1993;194:314–31.
- [15] Wotton D, Ghysdael J, Wang S, Speck NA, Owen MJ. Cooperative binding of Ets-1 and core binding factor to DNA. *Mol Cell Biol* 1994;14:840–50.
- [16] Giese K, Kingsley C, Kirshner JR, Grosschedl R. Assembly and function of a TCR $\alpha$  enhancer complex is dependent on LEF-1-induced DNA bending and multiple protein–protein interactions. *Genes Dev* 1995;9:995–1008.
- [17] Fitzsimmons D, Hodsdon W, Wheat W, Maira SM, Wasyluk B, Hagman J. Pax-5 (BSAP) recruits Ets proto-oncogene family proteins to form functional ternary complexes on a B-cell-specific promoter. *Genes Dev* 1996;10:2198–211.
- [18] Garvie CW, Hagman J, Wolberger C. Structural studies of Ets-1/Pax5 complex formation on DNA. *Mol Cell* 2001;8:1267–76.
- [19] Garvie CW, Pufall MA, Graves BJ, Wolberger C. Structural analysis of the autoinhibition of Ets-1 and its role in protein partnerships. *J Biol Chem* 2002;277:45529–36.
- [20] Wasyluk C, Gutman A, Nicholson R, Wasyluk B. The c-Ets oncoprotein activates the stromelysin promoter through the same elements as several non-nuclear oncoproteins. *EMBO J* 1991;10:1127–34.
- [21] Lamber EP, Vanhille L, Textor LC, Kachalova GS, Sieweke MH, Wilmanns M. Regulation of the transcription factor Ets-1 by DNA-mediated homo-dimerization. *EMBO J* 2008;27:2006–17.
- [22] Babayeva ND, Wilder PJ, Shiina M, Mino K, Desler M, Ogata K, et al. Structural basis of Ets1 cooperative binding to palindromic sequences on stromelysin-1 promoter DNA. *Cell Cycle* 2010;9:3054–62.
- [23] Rabault B, Ghysdael J. Calcium-induced phosphorylation of ETS1 inhibits its specific DNA binding activity. *J Biol Chem* 1994;269:28143–51.
- [24] Liu H, Grundström T. Calcium regulation of GM-CSF by calmodulin-dependent kinase II phosphorylation of Ets1. *Mol Biol Cell* 2002;13:4497–507.
- [25] Eyquem S, Chemin K, Fasseu M, Bories JC. The Ets-1 transcription factor is required for complete pre-T cell receptor function and allelic exclusion at the T cell receptor beta locus. *Proc Natl Acad Sci U S A* 2004;101:15712–7.
- [26] Moisan J, Grenningloh R, Bettelli E, Oukka M, Ho IC. Ets-1 is a negative regulator of Th17 differentiation. *J Exp Med* 2007;204:2825–35.
- [27] Hollenhorst PC, Chandler KJ, Poulsen RL, Johnson WE, Speck NA, Graves BJ. DNA specificity determinants associate with distinct transcription factor functions. *PLoS Genet* 2009;5:e1000778.
- [28] Kim WY, Sieweke M, Ogawa E, Wee HJ, Englmeier U, Graf T, et al. Mutual activation of Ets-1 and AML1 DNA binding by direct interaction of their autoinhibitory domains. *EMBO J* 1999;18:1609–20.
- [29] Goetz TL, Gu TL, Speck NA, Graves BJ. Auto-inhibition of Ets-1 is counteracted by DNA binding cooperativity with core-binding factor  $\alpha$ 2. *Mol Cell Biol* 2000;20:81–90.
- [30] Hagman J, Grosschedl R. An inhibitory carboxyl-terminal domain in Ets-1 and Ets-2 mediates differential binding of ETS family factors to promoter sequences of the *mb-1* gene. *Proc Natl Acad Sci U S A* 1992;89:8889–93.
- [31] Lim F, Kraut N, Frampton J, Graf T. DNA binding by c-Ets-1, but not v-Ets, is repressed by an intramolecular mechanism. *EMBO J* 1992;11:643–52.
- [32] Wasyluk C, Kerckaert JP, Wasyluk B. A novel modulator domain of Ets transcription factors. *Genes Dev* 1992;6:965–74.
- [33] Jonsen MD, Petersen JM, Xu QP, Graves BJ. Characterization of the cooperative function of inhibitory sequences in Ets-1. *Mol Cell Biol* 1996;16:2065–73.
- [34] Skalicky JJ, Donaldson LW, Petersen JM, Graves BJ, McIntosh LP. Structural coupling of the inhibitory regions flanking the ETS domain of murine Ets-1. *Protein Sci* 1996;5:296–309.
- [35] Kamberaj H, van der Vaart A. Correlated motions and interactions at the onset of the DNA-induced partial unfolding of Ets-1. *Biophys J* 2009;96:1307–17.
- [36] Petersen JM, Skalicky JJ, Donaldson LW, McIntosh LP, Alber T, Graves BJ. Modulation of transcription factor Ets-1 DNA binding: DNA-induced unfolding of an  $\alpha$  helix. *Science* 1995;269:1866–9.
- [37] Pufall MA, Lee GM, Nelson ML, Kang HS, Velyvis A, Kay LE, et al. Variable control of Ets-1 DNA binding by multiple phosphates in an unstructured region. *Science* 2005;309:142–5.
- [38] Tahirov TH, Inoue-Bungo T, Morii H, Fujikawa A, Sasaki M, Kimura K, et al. Structural analyses of DNA recognition by the AML1/Runx-1 Runt domain and its allosteric control by CBF $\beta$ . *Cell* 2001;104:755–67.
- [39] Wang H, McIntosh LP, Graves BJ. Inhibitory module of Ets-1 allosterically regulates DNA binding through a dipole-facilitated phosphate contact. *J Biol Chem* 2002;277:2225–33.
- [40] Wheat W, Fitzsimmons D, Lennox H, Krautkramer SR, Gentile LN, McIntosh LP, et al. The highly conserved  $\beta$ -hairpin of the paired DNA-binding domain is required for assembly of Pax-Ets ternary complexes. *Mol Cell Biol* 1999;19:2231–41.
- [41] Cowley DO, Graves BJ. Phosphorylation represses Ets-1 DNA binding by reinforcing autoinhibition. *Genes Dev* 2000;14:366–76.
- [42] Nghiem P, Saati SM, Martens CL, Gardner P, Schulman H. Cloning and analysis of two new isoforms of multifunctional Ca<sup>2+</sup>/calmodulin-dependent protein kinase. Expression in multiple human tissues. *J Biol Chem* 1993;268:5471–9.
- [43] Hollenhorst PC, Shah AA, Hopkins C, Graves BJ. Genome-wide analyses reveal properties of redundant and specific promoter occupancy within the ETS gene family. *Genes Dev* 2007;21:1882–94.
- [44] Klemm JD, Pabo CO. Oct-1 POU domain–DNA interactions: cooperative binding of isolated subdomains and effects of covalent linkage. *Genes Dev* 1996;10:27–36.

- 
- [45] Panne D, Maniatis T, Harrison SC. An atomic model of the interferon-beta enhanceosome. *Cell* 2007;129:1111–23.
- [46] Goodey NM, Benkovic SJ. Allosteric regulation and catalysis emerge via a common route. *Nat Chem Biol* 2008;4:474–82.
- [47] Boehr DD, Nussinov R, Wright PE. The role of dynamic conformational ensembles in biomolecular recognition. *Nat Chem Biol* 2009;5:789–96.
- [48] Hammes GG, Chang YC, Oas TG. Conformational selection or induced fit: a flux description of reaction mechanism. *Proc Natl Acad Sci U S A* 2009;106:13737–41.
- [49] Shrivastava T, Mino K, Babayeva ND, Baranovskaya OI, Rizzino A, Tahirov TH. Structural basis of Ets1 activation by Runx1. *Leukemia* 2014. <http://dx.doi.org/10.1038/leu.2014.111>.
- [50] Sigvardsson M, Clark DR, Fitzsimmons D, Doyle M, Åkerblad P, Breslin T, et al. Early B-cell factor, E2A, and Pax-5 cooperate to activate the early B cell-specific mb-1 promoter. *Mol Cell Biol* 2002;22:8539–51.
- [51] Baillat D, Bègue A, Stéhelin D, Aumercier M. ETS-1 transcription factor binds cooperatively to the palindromic head to head ETS-binding sites of the stromelysin-1 promoter by counteracting autoinhibition. *J Biol Chem* 2002;277:29386–98.
- [52] Nagaleekar VK, Diehl SA, Juncadella I, Charland C, Muthusamy N, Eaton S, et al. IP3 receptor-mediated Ca<sup>2+</sup> release in naive CD4 T cells dictates their cytokine program. *J Immunol* 2008;181:8315–22.